Investigation on motion responses of a semi-submersible platform and its mooring system

Yuan-chuan Liu[1, 2], De-cheng Wan[1], Qing Xiao[2*] and Atilla Incecik[2]

1. State Key Laboratory of Ocean Engineering, School of Naval Architecture, Ocean and Civil Engineering, Shanghai Jiao Tong University, Shanghai, 200240, China

2. Department of Naval Architecture, Ocean and Marine Engineering, University of Strathclyde, Glasgow, G4 0LZ, UK

Abstract: More and more floating structures are used in both offshore and coastal engineering, and also under assessment for wind energy. Mooring systems are needed by floating structures for station-keeping. In this paper, motion responses of a semi-submersible platform in regular waves are investigated numerically by a viscous flow solver naoe-FOAM-SJTU based on OpenFOAM. Influence of the mooring system on the motion responses of platform is evaluated via the study on (a) effect of each element length while maintaining the overall length as a constant; and (b) the cross angles between mooring lines.

Keywords: motion responses; semi-submersible platforms; mooring systems; OpenFOAM; naoe-FOAM-SJTU
Article ID: 1671-9433(2010)01-0000-00

1 Introduction

Floating structures are widely used in recent years not only as equipment for the exploration and exploitation of deep-water oil and gas in traditional ocean engineering industry, like semi-submersible platforms, Spars and Tension Leg Platforms (TLP), but also as facilities reducing waves like floating breakwaters in coastal engineering. Recently renewable energy companies are building floating offshore wind turbines in sea more than 30m deep. The reasons may vary but decreasing cost while increasing profits is always among the main causes for all industries. Unlike their counterparts with fixed bottoms, these floating structures need be equipped with essential mooring systems to help resist motion responses induced by environmental loads from continuous wind, wave and current at sea, and maintain their position within certain limits in order to function properly. Therefore, investigation of mooring systems, especially their effects on moored structures, has great significance for the design of floating structures.

Many researches have been done over recent years concerning the effects of mooring systems on floating structures in different aspects and some are focused on modeling methods of mooring lines. Waris and Ishihara (2012) investigated the applicability of linear and nonlinear FEM mooring models for both tension leg mooring and catenary mooring systems of floating offshore wind turbine systems. Results showed a good agreement for tension leg mooring while surge response was overestimated by the linear model for catenary mooring systems. Sethuraman and Venugopal (2013)demonstrated that an accurate modeling of mooring line dynamics with non-linearity and damping has to be employed when assessing the coupled hydrodynamic response of a 1:100 scale model of a floating stepped-spar wind turbine under regular and irregular waves. Kim et al. (2013) compared the dynamic coupled behavior of moored floating structures in time domain using two methods for mooring lines -- the linear spring method and the nonlinear FEM. It was found that the transient motion responses of structures was influenced by the adoption of FEM due to its inclusion of mooring damping. Effects of mooring system configuration such as the number, length and position of mooring lines were also discussed. Diamantoulaki and Angelides (2011) carried out a parametric study regarding effects of the number of mooring lines on performance of the cable-moored array of floating breakwaters under monochromatic linear waves in the frequency domain. Increasing number of lines seemed to exert little influence on the heave motion of the breakwaters. Sun et al. (2012) investigated the performance of a moored Spar platform and its mooring system under three different mooring configurations using a 3D hydrodynamic finite element model. The cross angle between lines was assigned 5, 10 and 15 degrees respectively. It concluded that as the cross angle increased, motion response of the platform decreased while line tension increased. Jeon et al. (2013) studied the dynamic responses of the floating substructure of a rigid spar-type offshore wind turbine with catenary mooring cables with respect to the length and connection position of mooring cables. It showed that increasing length of mooring cables would decrease peak amplitudes in surge and pitch motions, and the motions could be minimized when mooring cables were connected to or slightly above the center of buoyancy. Besides, mooring types were discussed by some researchers. Seebai and Sundaravadivelu (2009) investigated experimentally the behavior of spar platform of a 5MW floating offshore wind turbine with taut and catenary mooring systems. The taut moored model showed smaller responses of both surge and heave than the catenary moored model. Qiao and Ou (2013) carried out researches on three different types of mooring systems, i.e. catenary, semi-taut and taut, of a semi-submersible platform using a 3D hydrodynamic finite element model. Natural periods, damping ratios, motion responses of the platform and mooring line tensions were compared.

***Corresponding author Email:** qing.xiao@strath.ac.uk

Most of the work on moored floating structures utilizes the potential flow theory in either frequency or time domain to deal with the fluid-structure interaction owing to its relatively high efficiency and good accuracy. However, when it comes to problems with strong nonlinear phenomena such as green water and slamming or vortex induced vibration of Spars, the traditional theory has its limitations. Computational Fluid Dynamics (CFD) method might be employed for its more realistic model especially when computing resources become more accessible now. In this paper, a viscous flow solver named naoe-FOAM-SJTU (Shen et al., 2013) for floating structures with mooring systems is presented, which is developed on the popular open source toolbox OpenFOAM. The solver is adopted to study motion response problems of a floating semi-submersible platform with a catenary mooring system in regular waves and the effects of the mooring system on its response. Mathematical equations and numerical methods are first described Parameters of the platform, mooring system together with computational domain are then presented. Validation tests are carried out subsequently to justify the numerical simulation. The effects of mooring system are later illustrated by comparing motion response of the platform when the mooring system is configured with different mooring line composition or different included angle between lines in the same group. Discussions and conclusions are finally made summarizing results obtained from this paper.

2 Mathematical equations

The present solver naoe-FOAM-SJTU is based on a built-in solver in OpenFOAM Mathematical formulae related to the solver are described as follows.

2.1 Governing equations

For transient, incompressible and viscous fluid, flow problems are governed by the Navier-Stokes equations:

$$\nabla \cdot \mathbf{U} = 0 \tag{1}$$

$$\frac{\partial \rho \mathbf{U}}{\partial t} + \nabla \cdot (\rho(\mathbf{U} - \mathbf{U}_g)\mathbf{U}) = -\nabla p_d - \mathbf{g} \cdot \mathbf{x} \nabla \rho + \nabla \cdot (\mu \nabla \mathbf{U}) + \mathbf{f}_\sigma \tag{2}$$

where $\mathbf{U}$ and $\mathbf{U}_g$ represent velocity of flow field and grid nodes separately; $p_d = p - \rho \mathbf{g} \cdot \mathbf{x}$ is dynamic pressure of flow field by subtracting the hydrostatic part from total pressure p; $\mathbf{g}$, ρ and μ denote the gravity acceleration vector, density and dynamic viscosity of fluid respectively; $\mathbf{f}_\sigma$ is surface tension which only takes effect at the free surface and equals zero elsewhere.

2.2 Free surface capturing

Volume of Fluid (VOF) method (Hirt and Nichols, 1981) is adopted in OpenFOAM to capture the free surface. Volume fraction function denoted as α is defined for every cell, representing the ratio of volume fluid occupies in each cell. Therefore, α follows the distribution below:

$$\begin{cases} \alpha = 0, & air \\ \alpha = 1, & water \\ 0 < \alpha < 1, & free\ surface \end{cases} \tag{3}$$

The volume fraction function α is governed by the following transport equation:

$$\frac{\partial \alpha}{\partial t} + \nabla \cdot [(\mathbf{U} - \mathbf{U}_g)\alpha] + \nabla \cdot [\mathbf{U}_r(1-\alpha)\alpha] = 0 \tag{4}$$

2.3 Wave generation and damping

The present solver incorporates a wave generation module which can model various types of wave such as linear waves, Stokes 2nd order waves, freak waves, solitary waves, etc. Waves are generated by specifying the free surface and velocity distribution of the inlet boundary with varieties of wave theories (Baudic et al., 2001), avoiding movement of the boundary. The linear wave theory is adopted in this paper.

A wave damping module is developed for the present solver, which sets up a wave damping zone (Larsen and Dancy, 1983), also known as sponge layer, near the outlet boundary to alleviate wave reflection. The sponge layer takes effect by adding an additional artificial viscous term as source term to the momentum equation. The new term is expressed as:

$$\mathbf{f}_s(x) = \begin{cases} -\rho \mathbf{U} \alpha_s \left(\dfrac{x - x_0}{L_s} \right)^2, & x > x_0 \\ \mathbf{0}, & x \le x_0 \end{cases} \tag{5}$$

where α_s is a dimensionless quantity defining damping strength for the sponge layer. Other variables could be explained through Figure 1: x denote the coordinate in x direction of grid cells; x_0 and L_s represent separately the position and length of the sponge layer.

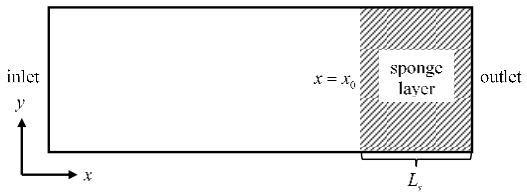

Figure 1 Sketch of sponge layer

2.4 Motion equations

The present solver integrates a 6DoF motion module capable of computing all six motion responses of a floating structure. Two coordinate systems, shown in Figure 2, are introduced to describe the motion pattern of structures: a global coordinate system for calculating forces and defining movements, and a local coordinate system for constructing motion equations. These two coordinate systems, as well as variables defined in them, can be related to each other via transformation matrices based on Euler angles (Carrica et al., 2007).

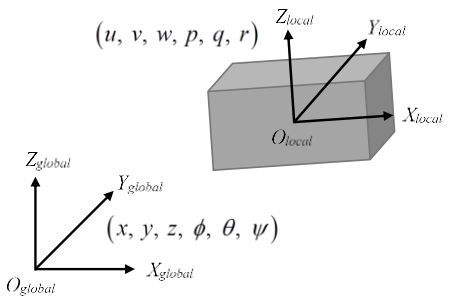

Figure 2 Definition of coordinate systems for 6DoF motion of a floating structure

2.5 Dynamic mesh deformation

Once motion of the structure is calculated, the whole computational mesh should be updated to manifest the impact of its new position on fluid field, which is achieved in OpenFOAM by employing the dynamic mesh deformation technique. Displacement of grid points $\mathbf{X}_g$ can be obtained via solving the following Laplace equation (Jasak and Tukovic, 2006):

$$\nabla \cdot \left(\gamma \nabla \mathbf{X}_g \right) = 0 \tag{6}$$

where $\gamma = 1/r^2$ represents the deformation coefficient and r is the distance from cell centers to boundaries of the structure.

2.6 Mooring system

The mooring system module here adopts the widely used three-dimensional lumped mass method (Huang, 1994) for dynamic analysis which employs a spring-mass model which discretize a continuous line into $N+1$ point masses (nodes) connected by N massless springs (segments). Considering the effect of acceleration, the dynamic equilibrium equation is built on nodes which can be illustrated in Figure 3:

$$M_i \vec{a}_i = \vec{F}_{Ti} - \vec{F}_{Ti-1} + \vec{F}_{Di} + \vec{F}_{Ai} - \vec{W}_i \tag{7}$$

where M_i and $\vec{a}_i$ are mass and acceleration vector of node i respectively; $\vec{F}_{Ti}$ and $\vec{F}_{Ti-1}$ are tension vectors of segments connected by node i; $\vec{F}_{Di}$ and $\vec{F}_{Ai}$ are drag and inertia forces distributed to node i from adjacent segments i and $i-1$ via averaging and calculated by Morison's equation; $\vec{W}_i$ is gravity of node i also obtained by means of averaging. The solving procedure is similar to the one proposed by Nakajima et al. (1982).

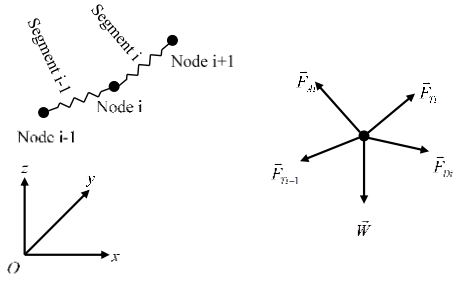

Figure 3 Force analysis of a node for lumped mass method

3 Computational model

A deep-water semi-submersible drilling platform with a catenary mooring system is selected in this paper, which was investigated both experimentally and numerically by Shi (2011). Parameters of both the platform and the mooring system are presented, as well as the computational domain used to carry out numerical simulations.

3.1 Platform parameters

The platform mainly consists of three parts as shown in

Figure 4Figure 4: a deck, four columns and two pontoons. The platform is symmetric with respect to both longitudinal and transverse sections at center plane. Principal parameters of the platform are listed in Table 1.

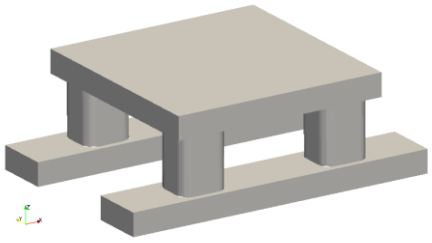

Figure 4 Sketch of a deep-water semi-submersible platform

Table 1 Principal parameters of the platform

Principal parameters	Unit	Value
Deck	m	78.68×78.68×8.60
Bottom of deck above baseline	m	30.0
Column	m	17.385×15.86×21.46
Fillet radius of column	m	3.96
Longitudinal distance between centerlines of columns	m	54.83
Transverse distance between centerlines of columns	m	58.56
Pontoon	m	114.07×20.12×8.54
Distance between centerlines of pontoons	m	58.56
Tonnage	t	51465.3
Center of gravity above baseline	m	24.26
Initial air gap	m	11.0
Draft	m	19.0
Roll gyration radius	m	33.3
Pitch gyration radius	m	32.4

3.2 Mooring system configuration

The mooring system is composed of 12 lines which are symmetrically arranged into 4 groups. Numbering and angles are shown in Figure 5 (a). Fairleads of all lines are positioned at the outside surface of the columns. All 12 lines share same parameters. Length of each line is 4300m, and it is made up of multi-component material which is connected through three parts with different length and material properties: the upper and lower parts are R4S chains while the middle part is polyester fiber cable, as shown in Figure 5 (b). Since water depth is 1,500m, the lines exhibit a catenary shape. The pretension acted on each line is 200t.

Main properties of a multi-component mooring line are listed in Table 2.

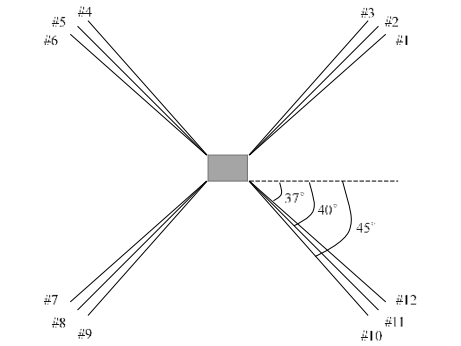

(a) Top view

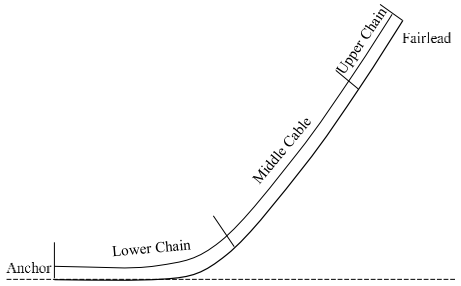

(b) Composition of a mooring line

Figure 5 Layout of mooring system for the platform

Table 2 Main properties of a multi-component mooring line

Position	Material	Length (m)	Diameter (mm)	Young's Modulus (Pa)	Weight in Water (N/m)
Upper	Chain	150	84	4.47756×10^{11}	1313.2
Middle	Cable	2650	160	4.67916×10^{10}	41.2
Lower	Chain	1500	84	4.47756×10^{11}	1313.2

3.3 Computational domain

A rectangular numerical tank is used and its size is L[-225m, 275m]×W[-150m, 150m]×H[-200m, 50m]. The platform is located at the center of the tank. Since the fluid field near free surface and the platform changes violently, cells are split locally for two or more times for better accuracy as in Figure 6. The ultimate cell number reaches up to nearly two million.

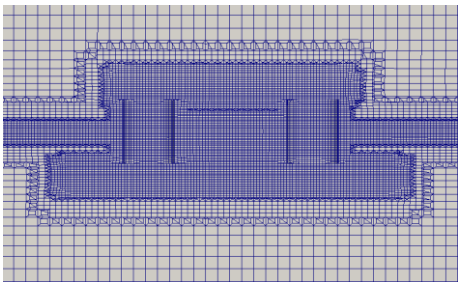

Figure 6 Local refinement for mesh near free surface

4 Validation

The present solver has been used to study problems of ship hydrodynamics and ocean engineering in various situations, such as wave generation and damping (Cha and Wan, 2011), wave run-up and impacts on fixed structures (Cao et al., 2011; Zhou et al., 2013), ship hydrodynamics and added resistance (Ye et al., 2012; Shen and Wan, 2013), motion response of moored floating platforms (Cao et al., 2013; Liu et al., 2013) and also sloshing (Shen and Wan, 2012).

In this paper, calculated results are compared to both experimental and numerical results from Shi (2011) to validate the capability of the present solver to handle hydrodynamic problems of moored offshore platforms in waves. Three regular incident waves are selected from model tests, parameters of which are listed in Table 3. Take the first wave as an example, and a wave gauge is located near the platform at X = -40m to record wave elevation. The curve of wave elevation is plotted in Figure 7, which shows that the wave changes regularly after about 6 periods with amplitude of 6m as prescribed and is thus satisfactory.

Table 3 Parameters of incident waves

Parameters/No.	1	2	3
Wave height (m)		6	
Wave period (s)	11.5	13	15.5
Wave length (m)	206.481	263.823	374.197

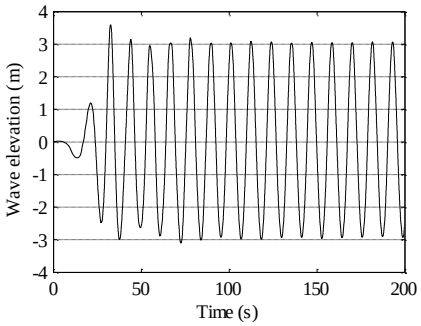

Figure 7 Elevation of incident wave (T = 11.5s, X = -40m)

Three numerical tests are set up associated with above mentioned three incident waves for validation. Incident waves propagate in the longitudinal direction of the platform, the movement is thus confined in its longitudinal section. As a result, only three degrees of freedom are considered, i.e., surge, heave and pitch, while others are fixed. The time step is fixed at 0.02s and the overall time simulated is set as 400s.

Figure 8 shows the comparison of Response Amplitude Operator (RAO) between numerical results and experimental data for surge, heave and pitch responses of the platform. The comparison shows that results from various means share the same trend, i.e., RAOs of surge and heave response decrease as the period of incident waves increases, while pitch response shows an opposite change pattern. Besides, values gained from white noise tests are larger than those of regular wave tests while present results by naoe-FOAM-SJTU, as well as those from SESAME, always stay between them. It can be then concluded that the present solver is capable of handling motion response problems of moored floating structures in waves.

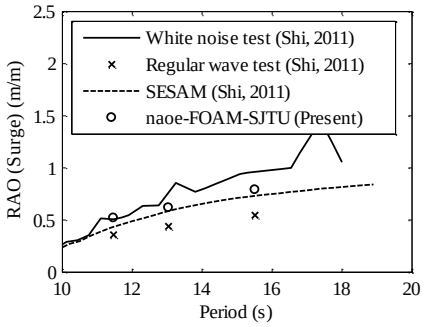

(a) Surge

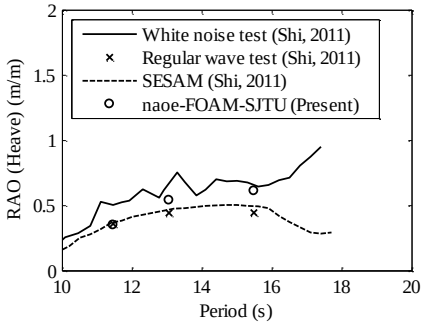

(b) Heave

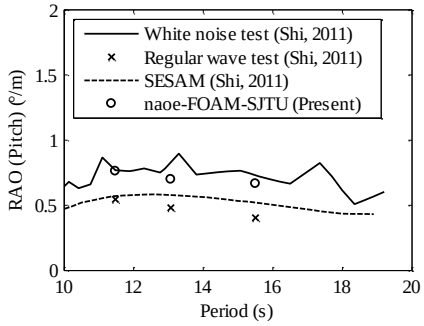

(c) Pitch

Figure 8 Comparison of RAOs for the platform

5 Numerical Results

In order to evaluate the influence of mooring system parameters on motion responses of the platform, two aspects are investigated: different mooring line compositions, i.e., varying length of each segment of the mooring line while keeping the overall length unchanged; different mooring system arrangements, namely the cross angles between mooring lines.

5.1 Effects of mooring line composition

For a multi-component mooring line, the length allocated to each component affects its shape and tension distribution, and may therefore exert an influence on the moored floating platform. In this section, two new configurations are set up for mooring lines by adjusting the length of different components shown in Figure 5 while maintaining the total length of the lines as 4300m and pretension as 200t. Parameters for all three configurations are listed in Table 4. For Case A, length of the upper chain increases while length of middle cable decreases; for Case B, length of the middle cable increases while length of the lower chain decreases.

Table 4 Parameters of different mooring line compositions

Configurations	Original	Case A	Case B
Upper chain length (m)	150	800	150
Middle cable length (m)	2650	2000	3150
Lower chain length (m)	1500	1500	1000

Figure 9 shows the shape of mooring lines with three different configurations at the initial state. Variation on the mooring line composition leads to rather evident changes of the shape. For Case A, these two parts connect with each other un-smoothly and the grounded part of the line increases as well. The included angle between the line and horizontal plane also becomes larger, meaning increased vertical tension provided to the moored platform and decreased horizontal tension when pretension remains the same. Case B shows the opposite change.

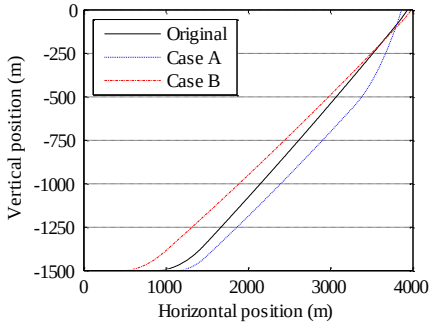

Figure 9 Shape of mooring lines with different compositions

To compare dynamic characteristics of the mooring system, fairleads move in the form of prescribed sinusoidal pattern: $x(t)=A\sin\left(\frac{2\pi}{T}\times t\right)$, where the amplitude of the movement is set as $A=6m$ and the period is $T=11.5s$. For the horizontal restoring force of mooring system shown in Figure 10, Case B and the original one look much alike while the magnitudes are reduced notably for Case A. Therefore, longer middle cable has little effect on loading of mooring system which however may be decreased by increasing upper chain of lines.

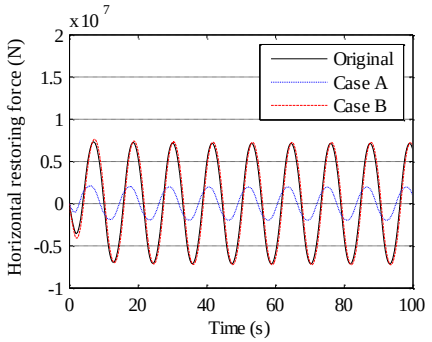

Figure 10 Comparison of horizontal restoring force of mooring system with different line compositions

Motion responses of two new configurations are calculated and then compared to the original configuration as shown in Figure 11. Only results between 250s and 400s are extracted to compute RAOs which are listed in Table 5. Results show the mooring line composition has influences on 3DoF motion responses of the platform to varying degrees.

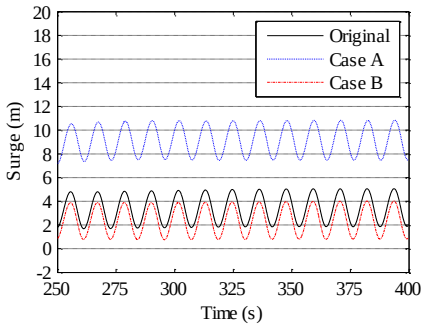

(a) Surge motion

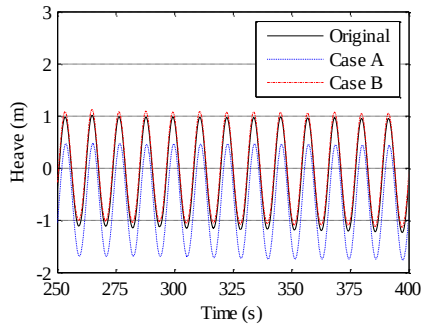

(b) Heave motion

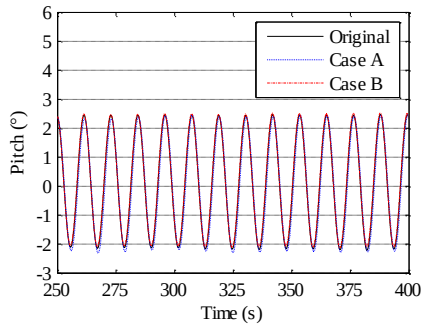

(c) Pitch motion

Figure 11 Comparison of motion responses of the platform with mooring system of different line compositions

Table 5 RAOs of the platform with mooring system of different mooring line compositions

Configurations	Original	Case A	Case B
Surge RAO（m/m）	0.5205	0.5521	0.5205
Heave RAO（m/m）	0.3523	0.3604	0.3523
Pitch RAO（°/m）	0.7612	0.7716	0.7566

For surge motion, when length of the upper chain increases, its RAO is larger accordingly and the mean position deviates farther reaching almost 9m, which is caused by smaller dynamic mooring loading. Increasing length of the middle cable, on the other hand, does not change the RAO but relatively larger dynamic mooring loading restricts drift movement a bit. For heave motion, the configuration of Case A leads to a slight increase of its RAO while the mean position falls under the initial draft since the vertical component of pretension alters the floating status of the platform. On the contrary, RAO remains nearly unchanged for Case B and the mean position rises slightly for a similar reason. For pitch motion, three curves are rather close and RAOs are also quite similar.

5.2 Effects of mooring system arrangement

Mooring systems are generally arranged into several groups of lines with identical properties. When the number of lines is fixed, cross angles between groups or lines in one group can change, resulting in different characteristics of the mooring system. In order to study the effects of mooring system arrangement, two new configurations are built by either decreasing or increasing the cross angles between mooring lines in one group, which are depicted in Figure 12.

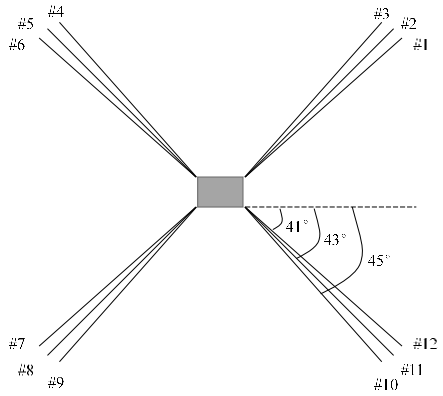

(a) Decrease angle between lines in one group

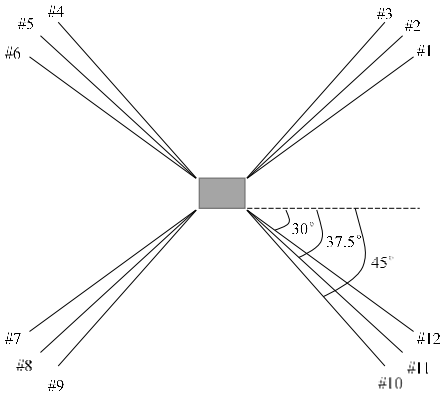

(b) Increase angle between lines in one group

Figure 12 Sketches of mooring system arrangements

Figure 13 shows curves of horizontal restoring force for different mooring system arrangements with respect to time. Three curves are rather close but increasing included angles can bring about larger horizontal restoring force which, known from conclusions in section 5.1, will restrict surge motion. It may thus be inferred that larger included angles will be favorable.

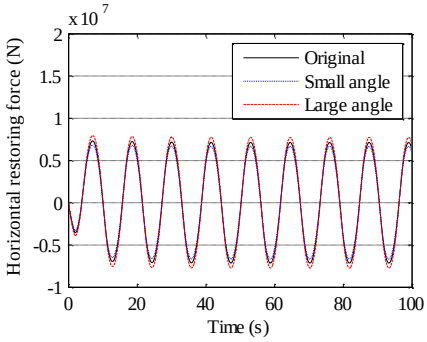

Figure 13 Horizontal restoring force for different mooring system arrangements

Simulations are carried out for the two new configurations and motion responses are shown in Figure 14. RAOs are computed and listed in Table 6. Results indicate that only the mean position of surge motion is influenced by the mooring system arrangements while other parameters are so close that their difference may be neglected. The inference made in last paragraph can also be verified, i.e., increasing included angles will prevent the platform from drifting further and therefore may be used for improving surge response.

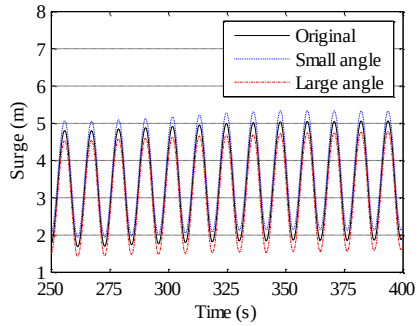

(a) Surge motion

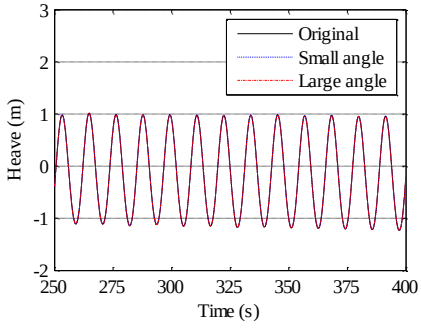

(b) Heave motion

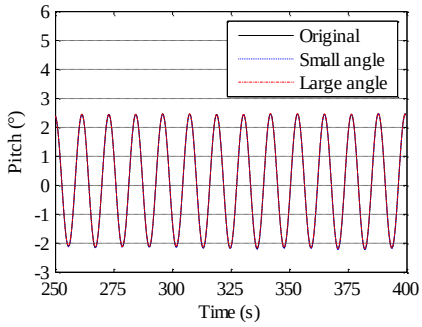

(c) Pitch motion

Figure 14 Comparison of motion responses of the platform with different mooring system arrangements

Table 6 RAOs of the platform with mooring system of different arrangements

Configurations	Original	Small angle	Large angle
Surge RAO（m/m）	0.5205	0.5217	0.5192
Heave RAO（m/m）	0.3523	0.3531	0.3513
Pitch RAO（°/m）	0.7612	0.7626	0.7595

6 Conclusions

In this paper, a viscous flow CFD solver based on the open source toolbox OpenFOAM is developed and presented. By comparing calculated results with those obtained from model tests, the ability of present solver to handle hydrodynamic problems of floating structures with mooring systems in waves is validated. The solver is then adopted to investigate effects of the mooring system on surge, heave and pitch responses of a semi-submersible platform in viscous fluid. Two sets of numerical simulation are carried out regarding different mooring line compositions and different mooring system arrangements. Conclusions can be drawn as follows:

1. Mooring systems have little influence on heave and pitch responses and relatively large effects on surge response, especially the low frequency drift motion.
2. Increasing the length of the middle cable of the multi-component mooring line while maintaining total length can suppress surge response. This configuration may thus be adopted if line tension limit can be satisfied.
3. Increasing the included angles between mooring lines in the same group of the mooring system can reduce the drift of the platform. As a result, this may be used as an improved configuration.

Although the application of present solver in this paper is limited to regular waves, it can be extended to irregular or extreme waves afterwards. Work done in this paper can be served as the foundation of future study for hydrodynamic problems such as slamming and green water phenomena of floating structures, as well as VIV of Spar platforms.

References

Baudic SF, Williams AN, Kareem A (2001). A Two-Dimensional Numerical Wave Flume—Part 1: Nonlinear Wave Generation, Propagation, and Absorption. *Journal of Offshore Mechanics and Arctic Engineering*, **123**(2), 70-75.

Cao H, Wang X, Liu Y, Wan D (2013). Numerical Prediction of

Wave Loading on a Floating Platform Coupled with a Mooring System. *The Twenty-third International Offshore and Polar Engineering Conference*, Anchorage, Alaska, USA, 582-589.

Cao H, Zha J, Wan D (2011). Numerical simulation of wave run-up around a vertical cylinder. *Proceedings of the Twenty-first (2011) International Offshore and Polar Engineering Conference, Maui, Hawaii, USA*, 726-733.

Carrica PM, Wilson RV, Noack RW, Stern F (2007). Ship motions using single-phase level set with dynamic overset grids. *Computers & Fluids*, **36**(9), 1415-1433.

Cha J, Wan D (2011). Numerical wave generation and absorption based on OpenFOAM. *The Ocean Engineering*, **29**(3), 1-12.

Diamantoulaki I, Angelides DC (2011). Modeling of cable-moored floating breakwaters connected with hinges. *Engineering Structures*, **33**(5), 1536-1552.

Hirt CW, Nichols BD (1981). Volume of fluid (VOF) method for the dynamics of free boundaries. *Journal of Computational Physics*, **39**(1), 201-225.

Huang S (1994). Dynamic analysis of three-dimensional marine cables. *Ocean Engineering*, **21**(6), 587-605.

Jasak H, Tukovic Z (2006). Automatic mesh motion for the unstructured finite volume method. *Transactions of FAMENA*, **30**(2), 1-20.

Jeon SH, Cho YU, Seo MW, Cho JR, Jeong WB (2013). Dynamic response of floating substructure of spar-type offshore wind turbine with catenary mooring cables. *Ocean Engineering*, **72**, 356-364.

Kim BW, Sung HG, Kim JH, Hong SY (2013). Comparison of linear spring and nonlinear FEM methods in dynamic coupled analysis of floating structure and mooring system. *Journal of Fluids and Structures*, **42**, 205-227.

Larsen J, Dancy H (1983). Open boundaries in short wave simulations—a new approach. *Coastal Engineering*, **7**(3), 285-297.

Liu Y, Sun R, Cao H, Wan D (2013). Motion response analysis of a semi-submersible platform with catenary mooring system. *Proceedings of the Eighth International Workshop on Ship Hydrodynamics*, Seoul, Korea.

Nakajima T, Motora S, Fujino M (1982). On the dynamic analysis of multi-component mooring lines. *Offshore Technology Conference*, 105-120.

Qiao D, Ou J (2013). Global responses analysis of a semi-submersible platform with different mooring models in South China Sea. *Ships and Offshore Structures*, **8**(5), 441-456.

Rusche H (2002). *Computational Fluid Dynamics of Dispersed Two-phase Flows at High Phase Fractions*. Doctoral Dissertation, University of London, London.

Seebai T, Sundaravadivelu R (2009). Effect of Taut And Catenary Mooring On Spar Platform With 5MW Wind Turbine. *The Eighth (2009) ISOPE Ocean Mining Symposium*, Chennai, India, 52-58.

Sethuraman L, Venugopal V (2013). Hydrodynamic response of a stepped-spar floating wind turbine: Numerical modelling and tank testing. *Renewable Energy*, **52**, 160-174.

Shen Z, Cao H, Ye H, Liu Y, Wan D (2013). Development of CFD Solver for Ship and Ocean Engineering Flows. *8th International OpenFOAM Workshop*, Jeju, Korea.

Shen Z, Wan D (2012). Numerical Simulations of Large-Amplitude Motions of KVLCC2 with Tank Liquid Sloshing in Waves. *2nd International Conference on Violent Flows*, Nantes, France, 149-156.

Shen Z, Wan D (2013). RANS Computations of Added Resistance and Motions of a Ship in Head Waves. *International Journal of Offshore and Polar Engineering*, **23**(4), 263-271.

Shi Q (2011). *Research on kinetic and dynamic characteristics of a deepwater drilling semi-submersible platform*. Master's Thesis, Shanghai Jiao Tong University, Shanghai, China. (In Chinese)

Sun JW, Fan XT, Wan XZ, Liu SX (2012). Numerical Study on Hydrodynamic Behavior of Deepwater Spar Platform with Different Mooring Configurations. *Applied Mechanics and Materials*, **137**, 50-58.

Waris MB, Ishihara T (2012). Dynamic response analysis of floating offshore wind turbine with different types of heave plates and mooring systems by using a fully nonlinear model. *Coupled Systems Mechanics*, **1**(3), 247-268.

Ye H, Shen Z, Wan D (2012). Numerical prediction of added resistance and vertical ship motions in regular head waves. *Journal of Marine Science and Application*, **11**(4), 410-416.

Zhou H, Cao H, Wan D (2013). Numerical Predictions of Wave Impacts on the Supporting Structures of Shanghai Donghai-Bridge Offshore Wind Turbines. *The Twenty-third International Offshore and Polar Engineering Conference*, Anchorage, Alaska, USA, 216-224.